RSC Advances

ROYAL SOCIETY OF CHEMISTRY

www.rsc.org/advances

Hydrogenation-Induced Large-Gap Quantum-Spin-Hall Insulator States in Germanium-Tin Dumbbell Structure

Xin Chen, Linyang Li, Mingwen Zhao*

School of Physics and State Key Laboratory of Crystal Materials, Shandong University, Jinan, Shandong, 250100, China

Abstract: The quantum spin Hall (QSH) effect in two-dimensional topological insulators (2D TIs) is promising for building nanoscaled devices with low energy consumption. The 2D TIs with a bulk band gap larger than the atomic thermal motion energy at room temperature (~26 meV) are essential for achieving room-temperature QSH effects. We proved from first-principles that this goal may be reached in a hydrogenated germanium-tin ($Sn_6Ge_4H_4$) dumbbell (DB) structure, where spin-orbit coupling (SOC) opens a bulk band gap of 235 meV. The topological nontriviality is related to the band inversion of s-p_{xy} of Sn atoms induced by surface hydrogenation and can be characterized by a topological invariant of Z_2=1. This work offers a promising candidate material for achieving long-desired room-temperature QSH effect.

Corresponding author, E-mail: zmw@sdu.edu.cn

Introduction

Topological insulators (TIs) are a new quantum state of matter with a topologically nontrivial bulk band gap due to spin-orbit coupling (SOC) and gapless surface or edge states. Protected by time-reversal symmetry, low-energy scattering of the edge states in two-dimensional (2D) TIs (also called quantum spin Hall (QSH) insulators) is enjoined, resulting in dissipationless transport edge channels[1-9], which are quite promising for application in spintronics and quantum computations. To achieve such application, the bulk band gap in TIs should be larger than the atomic thermal motion energy. Although many materials have been predicted to be QSH insulators, only HgTe/CdTe[10] and InAs/GaSb[11] quantum wells were verified by transport experiments at extremely low temperature, due to their small bulk gap. Increasing the critical temperature is highly desirable for achieving the QSH effect at room-temperature. This has motivated an intensive search for large-gap 2D QSH insulators, such as metal-organic frameworks[12-15] and those containing heavy metal atoms[16-20]. Additionally, our recent work showed that tensile strain can serve as an effective means to drive a normal insulator to a QSH insulator[21].

Inspired by the successful discovery and application of graphene, extensive research into the 2D group-IV materials has been conducted, and many exotic electronic properties have been revealed.[22-29] For example, low-buckled (LB) silicene, germanene and stanene[30] and their derivatives[31,32] have been reported as QSH insulators with relatively strong SOC. Some of them have a bulk gap larger than the thermal motion energy at room temperature (~26 meV). Apart from the LB

configurations with weak π-π bonding, a dumbbell (DB) structure was proposed as a stable phase of group-IV films[33-36]. Due to the fourfold-coordinated atoms included in this DB configuration, it is energetically more favorable than the LB configuration for some 2D group-IV materials[33,35,37-40], such as DB silicene and DB germanene. The plausibility of these DB configurations has also been evidenced by some experimental findings. For example, the $\sqrt{3} \times \sqrt{3}$ silicene multi-layers grown on an Ag(111) substrate[41,42,43] can be reproduced by stacking DB-based silicene derivatives[35, 44]. The 2×2 superstructure of germanene grown on an Al(111) substrate resembles DB germanene very well[45].

More interestingly, the DB configuration of tin (DB stanene) has been predicted to be a QSH insulator with a large topologically nontrivial bulk band gap[33,46], especially when it is hydrogenated (DB stanane)[46]. These works enrich the database of group-IV QSH insulators, beyond the LB honeycomb lattices, such as silicene, germanene, δ-graphyne[47], graphene nanomesh[48], stanene[33], etc. However, the topological nontriviality is not retained in all the DB configurations of 2D group-IV materials. For example, the DB germanene proposed by Özçelik et al.[40], is a normal insulator. Moreover, group-IV elements can form abundant compounds with one another, e.g. silicon-carbide (SiC), silicon-germanium (SiGe), germanium-tin (SnGe), and so on. The honeycomb lattice of silicon carbide with a stoichiometry of SiC_3 or Si_3C has been predicted to be QSH insulators[25]. However, the group-IV binary compounds with DB configurations have never been investigated so far. Whether they are QSH insulators remains unclear.

In this contribution, we reported our systematic study on the electronic structures of group-IV DB binary compounds (as shown in Fig.1a) from first-principles calculations. We found that in contrast to DB stanene, none of them are QSH insulators. However, upon hydrogenation, germanium-tin (Sn_6Ge_4) can be tuned to a QSH insulator characterized by a topological invariant of $Z_2 = 1$. The quantum phase transition was attributed to the band inversion of s-p_{xy} of Sn atoms induced by surface hydrogenation. The nontrivial bulk band gap in hydrogenated DB Sn_6Ge_4 ($Sn_6Ge_4H_4$) is about 235 meV, much larger than that of DB stanane[46] and the thermal motion energy (~ 26 meV) at room temperature. The phonon spectrum confirms the high stability and plausibility of DB $Sn_6Ge_4H_4$. This work offers a promising candidate material for applications of QSH effect at high temperature.

Methods

We preformed first-principles calculations within density-functional theory (EFT) using the plane wave basis Vienna ab initio simulation package known as VASP code[49-51]. The energy cutoff of the plane waves was set to 600 eV with an energy precision of 10^{-5} eV. A generalized gradient approximation (GGA) in the form proposed by Perdew, Burke, and Ernzerhof (PBE)[52] was adopted to treat the electron exchange-correlation functional. The atomic positions were relaxed until the maximum force on each atom was less than 0.01 eV/Å. The Brillouin zone (BZ) of the 2D materials was sampled by using an 11×11×1 Gamma-centered Monkhorst-Pack grid. A vacuum space of up to 20 Å was applied to minimize the artificial interactions between neighboring slabs. SOC was included by a second

variational procedure on a fully self-consistent basis. The phonon spectra were calculated using a supercell approach within the PHONON code[53].

Results and Discussion

The schematic representation of the DB configurations of group-IV binary compounds is shown in Fig. 1(a). Taking germanium-tin as an example, Sn and Ge have different coordination numbers, resulting in a stoichiometry of Sn_6Ge_4 (denoted as DB Sn_6Ge_4 hereafter). Sn is fourfold coordinated, similar to the case in stannane molecules (SnH_4), while Ge is only threefold coordinated with a dangling bond as in the case of LB germanene. All the Sn atoms are on the middle plane sandwiched by two planes of Ge atoms. The buckling height of the 2D hexagonal structure is about 3.11 Å, shorter than that of DB stanene, 3.41 Å. The lattice constant (the length of the base vectors) is 8.83Å. According to the electron localization function (ELF)[54, 55] profile shown in Fig. 1(a), despite the Ge-Sn covalent bonds, there are obvious regions of electron density in between the Ge atoms of the up- and down-planes, which are beneficial to the stabilization of the system. The length of the Ge-Sn bond is about 2.72 Å. The distance between the two Ge planes is about 3.11 Å, longer than that in germanene, 2.44Å.

To evaluate the energetic stability of DB Sn_6Ge_4, we calculated the formation energy (E_{form}) with respect to LB germanene and stanene, according to the expression: $E_{form} = (E_{total} - n_{Ge}\times\mu_{Ge} - n_{Sn}\mu_{Sn})/(n_{Ge} + n_{Sn})$, where E_{total} is the total energy per unit cell of DB Sn_6Ge_4, μ_{Ge} and μ_{Sn} are the chemical potentials of Ge and Sn atoms in the already-synthesized LB germanene and stanene[30], n_{Ge} are the respective numbers of

the Ge and Sn atoms in one unit cell of DB Sn_6Ge_4. Our DFT calculations showed that DB Sn_6Ge_4 has a negative formation energy of about -0.14 eV/atom, suggesting the energetically favorability over LB germanene and stanene. The energetic stability of DB Sn_6Ge_4 is related to its unique coordination. The fourfold coordinated Sn and the interaction between the up- and down-planes of the threefold coordinated Ge atoms contribute to the stability of DB Sn_6Ge_4 over LB germanene and stanene composing exclusively of threefold coordinated Sn or Ge atoms[33-36]. By ab initio phonon spectrum calculations, we further demonstrated the dynamic stability of DB Sn_6Ge_4, as shown in Fig. 1(b). No modes with imaginary frequencies were found in the spectrum and the structure was therefore proved to be dynamically stable.

The electronic band structures of DB Sn_6Ge_4 were then calculated. Without considering SOC, the band lines in the vicinity of the Fermi level, as indicated in Fig. 2 (a), exhibit a direct band gap of 242 meV at the Γ point. When SOC was switched on, the direct-band-gap features were preserved, but the band gap was narrowed to 64 meV, as shown in Fig 2(b). Parity analysis indicates that this is topological trivial band gap with a zero topological invariant (Z_2=0). Pristine DB Sn_6Ge_4 is therefore a normal insulator, similar to the bulk counterpart. We also calculated the electronic band structures of other group-IV binary compounds with DB configurations, DB X_6Y_4 (X,Y=C, Si, Ge, and Sn), and found that one of them are QSH insulators (see Supporting Information).

Ge atoms can be easily bonded with H atoms, for instance, in the case of germane (GeH_4). We tried to passivate the dangling bonds of Ge atoms in DB Sn_6Ge_4 with H

atoms. As shown in Fig. 3(a), all the Sn and Ge atoms in hydrogenated DB Sn_6Ge_4 (denoted as $Sn_6Ge_4H_4$ hereafter) are fully-coordinated. The H-Ge distance in the optimized $Sn_6Ge_4H_4$ is 1.56 Å, close to the value 1.55 Å in germane molecule. The distance between Ge planes is enlarged to 3.25Å. Both the lattice constant (8.75 Å) and the Ge-Sn distance (2.70 Å) are shorter than the corresponding values of pristine DB Sn_6Ge_4 (8.83Å and 2.72Å), respectively. The binding energy of hydrogen atoms with DB Sn_6Ge_4 is about -2.17 eV, lower than that in DB stanane, -1.92 eV[46]. These results confirmed that hydrogen atom can chemically bind to Ge atoms, in consistent with the ELF profile shown in Fig. 3(a). The Sn-Ge covalent bonds are retained in DB $Sn_6Ge_4H_4$, while the interaction between the up- and down-planes of Ge atoms is weakened as indicated by ELF profiles and the enlarged spacing between Ge planes.

To demonstrate the energetic stability of DB $Sn_6Ge_4H_4$, we compared the energy of DB $Sn_6Ge_4H_4$ with the sum of the energies of isolated DB Sn_6Ge_4 and atomic hydrogen atoms in hydrogen plasma environment[56, 57]. Our DFT calculations showed that the former is lower than the later by 0.62 eV/atom. The energetic favorability of DB $Sn_6Ge_4H_4$ can also be demonstrated by a hypothetical reaction: $6SnH_4 + 4GeH_4 \rightarrow Sn_6Ge_4H_4 + 18H_2$. Our calculation indicates that it is an exothermal reaction with an energy release of 0.15 eV/atom. The phonon spectrum of DB $Sn_6Ge_4H_4$ is plotted in Fig. 3(b). Obviously, there are no modes with imaginary frequencies, implying the dynamic stability of DB $Sn_6Ge_4H_4$.

The electronic band structure of DB $Sn_6Ge_4H_4$ differs significantly from that of pristine DB Sn_6Ge_4. Without considering SOC, DB $Sn_6Ge_4H_4$ is a gapless

semiconductor with the valence band maximum (VBM) and conduction band minimum (CBM) energetically degenerate at the Γ point, as shown in Fig. 4(a). The electronic states in the vicinity of the Fermi level originate from different atomic orbitals. The orbital-resolved electron density of states (DOS) showed that both VBM and CBM arise mainly from the $p_{x,y}$ atomic orbitals of the Sn atoms, as shown in Fig. 4 (b), in good consistent with the density profiles of the electron wavefunctions (WFs) shown in Fig. 4(d). For the valence band next to VBM (denoted as VBM-1), the WFs exhibit clear features of the s-orbital of Sn atoms and p_z-orbital of Ge atoms. The degeneracy of the two $p_{x,y}$ bands at the Γ point is a direct consequence of the C_{3v} symmetry of the lattice. Such band alignment represents a common feature of a QSH insulator family, including DB stanane[46] and the derivatives of germanene[31, 32], which is closely related to topological nontriviality. Further studies on other group-IV binary compounds indicated that none of them exhibit such type of band alignment (see Supporting Information). DB $Sn_6Ge_4H_4$ stands out from the group-IV binary compounds as a candidate QSH insulator.

When SOC was switched on in our DFT calculations, a band gap of 275 meV is opened up at the Γ point of DB $Sn_6Ge_4H_4$, as shown in the down panel of Fig. 4(a). The global indirect band gap is about 166 meV, slightly larger than that of DB stanane, 160 meV[46]. Such a large bulk gap suggests that DB $Sn_6Ge_4H_4$ is quite promising for achieving room-temperature QSH effect.

A comparison study of the orbital-resolved band structures of DB Sn_6Ge_4 and DB $Sn_6Ge_4H_4$ was then conducted to determine their topological aspects. For convenience,

we denoted the electronic states arising from s, $p_{x,y}$, p_z atomic orbitals of Sn as $|s^{\pm}>$, $|p_{x,y}^{\pm}>$ and $|p_z^{\pm}>$, in which the parity of the states are labeled by "+/−". For pristine DB Sn_6Ge_4, no matter whether SOC is included or not, the energies of the electronic states near the Fermi level are successively in the same order: $|p_{x,y}^{+}>$, $|p_z^{-}>$ and $|s^{-}>$, as shown in Fig. 5(a). But the order of $|p_{x,y}^{+}>$ and $|s^{-}>$ is reversed in DB $Sn_6Ge_4H_4$ without SOC, as shown Fig. 5(b), leading to a s-p_{xy}band inversion. When SOC was included, the degeneracy of the partial occupied $|p_{x,y}^{+}>$ state in DB $Sn_6Ge_4H_4$ was lifted, resulting in a large nontrivial band gap. This implies that surface hydrogenation induces the s-p_{xy} band inversion and drives DB Sn_6Ge_4 to a QSH insulator, as visually revealed in Fig. 5(c). Such s-p-type band inversion mechanism[59] also holds in other QSH insulators, such as HgTe quantum well[7] and fluorinated stanene[31].

The topological nontriviality of DB $Sn_6Ge_4H_4$ can be confirmed by a nonzero topological invariant Z_2. Because both DB Sn_6Ge_4 and DB $Sn_6Ge_4H_4$ have an inversion symmetry, the Z_2 index can be calculated using the parity criteria proposed by Fu and Kane[58]. According to this strategy, the Z_2 index can be determined from the parities of the four time-reversal and parity invariant points at BZ. The four time-reversal invariant momenta of the two lattices occur at the Γ and three M points, as shown in Fig. 5(d). The Z_2 invariant ν is defined by

$$(-1)^{\nu} = \prod_i \delta_i \text{ with } \delta_i = \prod_{m=1}^{N} \xi_{2m}(\Gamma_i)$$

for 2N occupied bands. $\xi_{2m}(\Gamma_i) = \pm 1$ is the parity eigenvalue of the *2m*-th occupied energy band at the time-reversal invariant momentum Γ_i. Our DFT calculations

showed that $\boldsymbol{\delta_i}$ has the values of (+), (+), (+), (+) in DB Sn_6Ge_4 and (+), (−), (−), (−) in DB $Sn_6Ge_4H_4$ at their four time-reversal invariant momenta, as indicated in Fig. 5(d). The topological invariants of pristine DB Sn_6Ge_4 and DB $Sn_6Ge_4H_4$ are therefore Z_2=0 and Z_2=1 respectively, suggesting the quantum phase transition from a normal insulator (DB Sn_6Ge_4) to a QSH insulator (DB $Sn_6Ge_4H_4$) induced by surface hydrogenation.

In view of the failure of PBE functional in determining electronic band gaps, we employed a hybrid functional in the form of Heyd-Scuseria-Ernzerhof (HSE) [60] to recalculate the electronic band structure of DB $Sn_6Ge_4H_4$. By incorporating a potion of exact exchange from Hartree-Fock (HF) theory, HSE functional can give band gaps comparable to experimental values. We found that the s-p band inversion and topological nontriviality of DB $Sn_6Ge_4H_4$ are retained even under a tensile stain. The bulk band gaps opened due to SOC are about 235 meV (indirect) and 317 meV (direct band gap at the Γ), both of which are much larger than the PBE results.

Substrates are inevitable in the fabrication procedure of QSH-insulator-based devices. However, the coupling between QSH insulators with substrates may destroy their topological nontriviality[20, 30]. For instance, when stanane is grown on a semiconducting substrate, it becomes a normal insulator or a metal without topological nontriviality[30]. To determine the influence of substrate on the topological nontriviality of DB $Sn_6Ge_4H_4$, we built a superstructure of DB $Sn_6Ge_4H_4$ on a $(\sqrt{12} \times \sqrt{12})$ h-BN substrate, as shown in Fig. 6(a). The lattice of DB $Sn_6Ge_4H_4$ matches well with that of the h-BN substrate with a difference less than 0.6%. At the

equilibrium state, the interlayer spacing between DB $Sn_6Ge_4H_4$ and the substrate is about 2.29 Å, suggesting weak interaction between them. We calculated the electronic band structure of the superstructure and found that the band lines in the vicinity of the Fermi level are in accordance with the free-standing DB $Sn_6Ge_4H_4$, as shown in Fig. 6(b) and 6(c). Both s-p band inversion and topological nontriviality are intact, except that the SOC bulk gap is slightly improved. The robust topological nontriviality of DB $Sn_6Ge_4H_4$ against substrate effects is related to the origins of the bands near the Fermi level. These bands are mainly contributed by s and p_{xy} atomic orbitals rather than p_z orbital and thus are unlikely affected by substrates.

Conclusions

Using first-principles calculations, we demonstrated theoretically that the unique coordinates of the 2D germanium-tin compound with a dumbbell structure (DB Sn_6Ge_4) make it energetically more stable than low-buckled stanene and germanene. DB Sn_6Ge_4 is a normal insulator with a direct gap of 242 meV. However, upon surface hydrogenation (resulting in DB $Sn_6Ge_4H_4$), it converts a QSH insulator characterized by a topological invariant of Z_2=1. The quantum phase transition from a normal insulator to a QSH insulator is related to the s-p band inversion induced by surface hydrogenation. The bulk band gap opened due to SOC can be as large as 235 meV which is much larger than the thermal motion energy at room temperature (~26 meV). The topological nontriviality is robust against substrate effects. The energetic stability and the phonon spectrum confirm the high stability and plausibility of DB $Sn_6Ge_4H_4$. These results are beneficial for achieving long-desired room-temperature QSH effect

and fabrication of high-speed spintronics devices.

Acknowledgements

This work is supported by the National Basic Research Program of China (No. 2012CB932302), the National Natural Science Foundation of China (No. 91221101, 21433006), the 111 project (No. B13029), the Taishan Scholar Program of Shandong, and the National Super Computing Centre in Jinan.

References

1 X. L. Qi and S. C. Zhang, Topological insulators and superconductors, *Rev. Mod. Phys.*, 2011, **83**, 1057.

2 B. A. Bernevig and S. C. Zhang, Quantum spin Hall effect, *Phys. Rev. Lett.*, 2006, **96**, 106802.

3 C. L. Kane and E. J. Mele, Quantum spin Hall effect in graphene, *Phys. Rev. Lett.*, 2005, **95**, 226801.

4 M. Z. Hasan and C. L. Kane, Colloquium: topological insulators, *Rev. Mod. Phys.*, 2010, **82**, 3045.

5 B. A. Bernevig, T. L. Hughes, and S. C. Zhang, Quantum spin Hall effect and topological phase transition in HgTe quantum wells, *Science*, 2006, **314**, 1757.

6 H. Weng, X. Dai, and Z. Fang, Transition-metal pentatelluride $ZrTe_5$ and $HfTe_5$: A paradigm for large-gap quantum spin Hall insulators, *Phys. Rev. X*, 2014, **4**, 011002.

7 C. L. Kane, and E. J. Mele, Z_2 topological order and the quantum spin Hall effect, *Phys. Rev. Lett.*, 2005, **95**, 146802.

8 C. Wu, B. A. Bernevig, and S. C. Zhang, Helical liquid and the edge of quantum spin Hall systems, *Phys. Rev. Lett.*, 2006, **96**, 106401.

9 C. Xu, and J. Moore, Stability of the quantum spin Hall effect: Effects of interactions, disorder, and Z_2 topology, *Phys. Rev. B*, 2006, **73**, 045322.

10 M. Konig, S. Wiedmann, C. Brune, A. Roth, H. Buhmann, L. W. Molenkamp, X. L. Qi, and S. C. Zhang, Quantum spin Hall insulator state in HgTe quantum wells,

Science, 2007, **318**, 766.

11 I. Knez, R. R. Du, and G. Sullivan, Evidence for helical edge modes in inverted InAs/GaSb quantum wells, *Phys. Rev. Lett.*, 2011, **107**, 136603.

12 Z. Liu, Z. F. Wang, J. W. Mei, Y. S. Wu, and F. Liu, Flat Chern band in a two-dimensional organometallic framework, *Phys. Rev. Lett.*, 2013, **110**, 106804.

13 L. Y. Li, X. M. Zhang, X. Chen, and M. W. Zhao, Giant topological nontrivial band gaps in chloridized gallium bismuthide, *Nano Lett.*, 2015, **15**, 1296.

14 Z. F. Wang, N. Su, and F. Liu, Prediction of a two-dimensional organic topological insulator, *Nano Lett.*, 2013, **13**, 2842.

15 Z. F. Wang, Z. Liu, and F. Liu, Quantum anomalous Hall effect in 2D organic topological insulators, *Phys. Rev. Lett.*, 2013, **110**, 196801.

16 Z. Liu, C. X. Liu, Y. S. Wu, W. H. Duan, F. Liu, and J. Wu, Stable nontrivial Z_2 topology in ultrathin Bi (111) films: a first-principles study, *Phys. Rev. Lett.*, 2011, **107**, 136805.

17 C. C. Liu, S. Guan, Z. G. Song, S. A. Yang, J. B. Yang, and Y. Yao, Low-energy effective Hamiltonian for giant-gap quantum spin Hall insulators in honeycomb X-hydride/halide (X= N–Bi) monolayers, *Phys. Rev. B*, 2014, **90**, 085431.

18 J. J. Zhou, W. Feng, C. C. Liu, S. Guan, and Y. Yao, Large-gap quantum spin Hall insulator in single layer bismuth monobromide Bi_4Br_4, *Nano Lett.*, 2014, **14**, 4767.

19 F. C. Chuang, L. Z. Yao, Z. Q. Huang, Y. T. Liu, C. H. Hsu, T. Das, H. Lin, and A. Bansil, Prediction of large-gap two-dimensional topological insulators consisting of bilayers of group III elements with Bi, *Nano Lett.*, 2014, **14**, 2505.

20 M. Zhou, W. Ming, Z. Liu, Z. Wang, P. Li, and F. Liu, Epitaxial growth of large-gap quantum spin Hall insulator on semiconductor surface, *Proc. Natl. Acad. Sci. USA*, 2014, **111**, 14378.

21 M. W. Zhao, X. Chen, L. Y. Li, and X. M. Zhang, Driving a GaAs film to a large-gap topological insulator by tensile strain, *Sci. Rep.*, 2015, **5**, 8441.

22 A. H. Castro Neto, N. M. R. Peres, K. S. Novoselov, and A. K. Geim, The electronic properties of graphene, *Rev. Mod. Phys.*, 2009, **81**, 109.

23 J. C. Charlier and S. Roche, Electronic and transport properties of nanotubes, Rev. Mod. Phys., 2007, 79, 677.

24 R. Rurali, Colloquium: Structural, electronic, and transport properties of silicon nanowires, *Rev. Mod. Phys.*, 2010, **82**, 427.

25 M. Zhao, and R. Zhang, Two-dimensional topological insulators with binary honeycomb lattices: Si C 3 siligraphene and its analogs, *Phys. Rev. B*, 2014, **89**, 195427.

26 L. Y. Li and M. W. Zhao, Structures, energetics, and electronic properties of multifarious stacking patterns for high-buckled and low-buckled silicene on the MoS_2 substrate, *J. Phys. Chem. C*, 2014, **118**, 19129.

27 L. Y. Li and M. W. Zhao, First-principles identifications of superstructures of germanene on Ag (111) surface and h-BN substrate, *Phys. Chem. Chem. Phys.*, 2013, **15**, 16853.

28 L. Y. Li, X. P. Wang, X. Y. Zhao, and M. W. Zhao, Moiré superstructures of silicene on hexagonal boron nitride: a first-principles study, *Phys. Lett. A*, 2013,

377, 2628.

29 H. Zhou, M. Zhao, X. Zhang, W. Dong, X. Wang, H. Bu, and A. Wang, First-principles prediction of a new Dirac-fermion material: silicon germanide monolayer, *J. Phys-Condens Mat.*, 2013, **25**, 395501.

30 F. Zhu, W. Chen, Y. Xu, C. Gao, D. Guan, C. Liu, D. Qian, S. C. Zhang, and J. Jia, Epitaxial growth of two-dimensional stanene, arXiv preprint arXiv:1506.01601, 2015.

31 Y. Xu, B. Yan, H. J. Zhang, J. Wang, G. Xu, P. Tang, W. Duan, and S. C. Zhang, Large-gap quantum spin Hall insulators in tin films, *Phys. Rev. Lett.*, 2013, **111**, 136804.

32 C. Si, J. Liu, Y. Xu, J. Wu, B. L. Gu, and W. Duan, Functionalized germanene as a prototype of large-gap two-dimensional topological insulators, *Phys. Rev. B*, 2014, **89**, 115429.

33 P. Tang, P. Chen, W. Cao, H. Huang, S. Cahangirov, L. Xian, Y. Xu, S. C. Zhang and W. Duan, A. Rubio, Stable two-dimensional dumbbell stanene: A quantum spin Hall insulator, *Phys. Rev. B*, 2014, **90**, 121408.

34 V. O. Özçelik and S. Ciraci, Local reconstructions of silicene induced by adatoms, *J. Phys. Chem. C*, 2013, **117**, 26305.

35 S. Cahangirov, V. O. Özçelik, L. Xian, J. Avila, S. Cho, M. C. Asensio, S. Ciraci, and A. Rubio, Atomic structure of the 3×3 phase of silicene on Ag (111), *Phys. Rev. B*, 2014, **90**, 035448.

36 D. Kaltsas and L. Tsetseris, Stability and electronic properties of ultrathin films of

silicon and germanium, *Phys. Chem. Chem. Phys.*, 2013, **15**, 9710.

37 S. Cahangirov, M. Topsakal, E. Aktürk, H. Sahin, and S. Ciraci, Two-and one-dimensional honeycomb structures of silicon and germanium, *Phys. Rev. Lett.*, 2009, **102**, 236804.

38 C. C. Liu, H. Jiang, and Y. Yao, Low-energy effective Hamiltonian involving spin-orbit coupling in silicene and two-dimensional germanium and tin, *Phys. Rev. B*, 2011, **84**, 195430.

39 C. C. Liu, W. Feng, and Y. Yao, Quantum spin Hall effect in silicene and two-dimensional germanium, *Phys. Rev. Lett.*, 2011, **107**, 076802.

40 V. O. Özcelik, E. Durgun, and S. Ciraci, New phases of germanene, *J. Phys. Chem. Lett.*, 2014, **5**, 2694

41 P. De Padova, P. Vogt, A. Resta, J. Avila, I. Razado-Colambo, C. Quaresima, C. Ottaviani, B. Olivieri, T. Bruhn, T. Hirahara, T. Shirai, S. Hasegawa, M. C. Asensio, and G. Le Lay, Evidence of Dirac fermions in multilayer silicone, *Appl. Phys. Lett.*, 2013, **102**, 163106.

42 P. Vogt, P. Capiod, M. Berthe, A. Resta, P. De Padova, T. Bruhn, G. Le Lay, and B. Grandidier, Synthesis and electrical conductivity of multilayer silicone, *Appl. Phys. Lett.*, 2014, **104**, 021602.

43 B. Feng, Z. Ding, S. Meng, Y. Yao, X. He, P. Cheng, L. Chen, and K. Wu, Evidence of silicene in honeycomb structures of silicon on Ag (111), *Nano Lett.*, 2012, **12**, 3507.

44 V. O. Özcelik, D. Kecik, E. Durgun, and S. Ciraci, Adsorption of group-IV

elements on graphene, silicene, germanene, stanene: dumbbell formation, *J. Phys. Chem. C*, 2015, **119**, 845

45 M. Derivaz, D. Dentel, R. Stephan, M. C. Hanf, A. Mehdaoui, P. Sonnet, and C. Pirri, Continuous germanene layer on Al (111), *Nano Lett.*, 2015, **15**, 2510.

46 X. Chen, L. Li, and M. Zhao, Dumbbell Stanane: A large-gap quantum spin Hall insulator, *Phys. Chem. Chem. Phys.*, 2015, DOI: 10.1039/C5CP00046G.

47 M. Zhao, W. Dong, and A. Wang, Two-dimensional carbon topological insulators superior to graphene, *Sci. Rep.*, 2013, **3**, 3532.

48 X. Zhang, and M. Zhao, Prediction of quantum anomalous Hall effect on graphene nanomesh, *RSC Adv.*, 2015,5, 9875-9880

49 G. Kresse and J. Furthmüller, Efficient iterative schemes for ab initio total-energy calculations using a plane-wave basis set, *Phys. Rev. B*, 1996, **54**, 11169.

50 G. Kresse and J. Hafner, Ab initio molecular dynamics for open-shell transition metals, *Phys. Rev. B*, 1993, **48**, 13115.

51 G. Kresse and D. Joubert, From ultrasoft pseudopotentials to the projector augmented-wave method, *Phys. Rev. B*, 1999, **59**,1758.

52 J. P. Perdew, K. Burke, and M. Ernzerhof, Generalized gradient approximation made simple, *Phys. Rev. Lett.*, 1996, **77**, 3865.

53 K. Parlinski, Z. Q. Li, and Y. Kawazoe, First-principles determination of the soft mode in cubic ZrO_2, *Phys. Rev. Lett.*, 1997, **78**, 4063.

54 A. D. Becke and K. E. Edgecombe, A simple measure of electron localization in atomic and molecular systems, *J. Chem. Phys.*, 1990, **92**, 5397.

55 A. Savin, O. Jepsen, J. Flad, O. K. Andersen, H. Preuss, and H. G. von Schnering, Electron localization in solid‐state structures of the elements: the diamond structure, *Angew. Chem. Int. Ed.*, 1992, **31**, 187.

56 Z. Sun, C. L. Pint, D. C. Marcano, C. Zhang, J. Yao, G. Ruan, Z. Yan, Y. Zhu, and R. H. Hauge, Towards hybrid superlattices in graphene, *Nat. Commun.*, 2011, **2**, 559.

57 M. Pumera and C. H. Wong, Graphane and hydrogenated graphene, *Chem. Soc. Rev.*, 2013, **42**, 5987.

58 L. Fu and C. L. Kane, Topological insulators with inversion symmetry, *Phys. Rev. B*, 2007, **76**, 045302.

59 H. Zhang and S. C. Zhang, Topological insulators from the perspective of first-principles calculations, *Phys. Status Solidi RRL*, 2013, **7**, 72.

60 J. Heyd, G. Scuseria, and M. Ernzerhof, Heyd-Scuseria-Ernzerhof hybrid functional for calculating the lattice dynamics of semiconductors, *J. Chem. Phys.*, 2013, **118**, 8207.

Figure caption

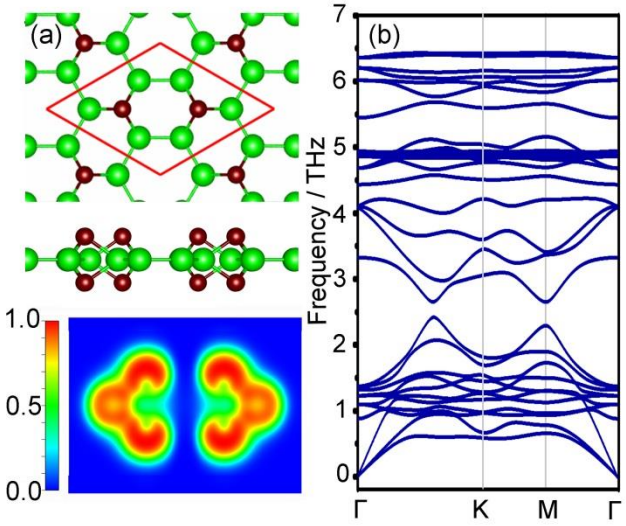

Figure 1. (a) Schematic representations (top and side views are presented in up and middle panels) and the ELF profiles (down panel) of DB Sn_6Ge_4. (b) Phonon spectrum of DB Sn_6Ge_4 along the high-symmetric points in the BZ.

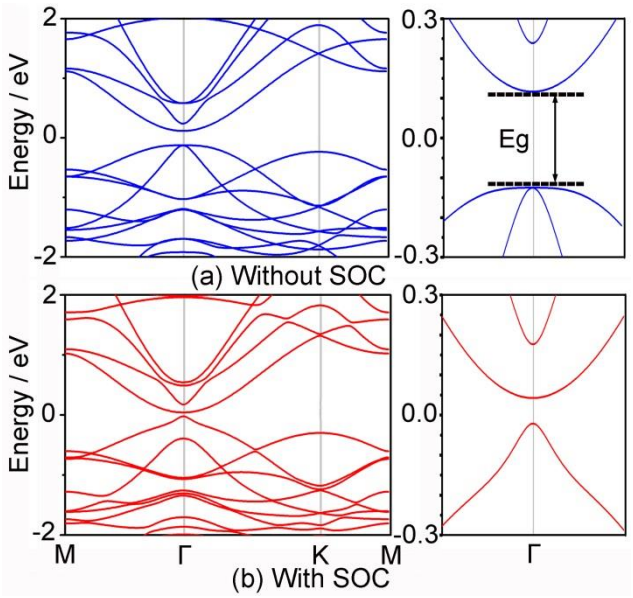

Figure 2. Band structures and their enlarged views (right panel) of DB Sn6Ge4 (a) without and (b) with SOC. The energy at the Fermi level was set to zero.

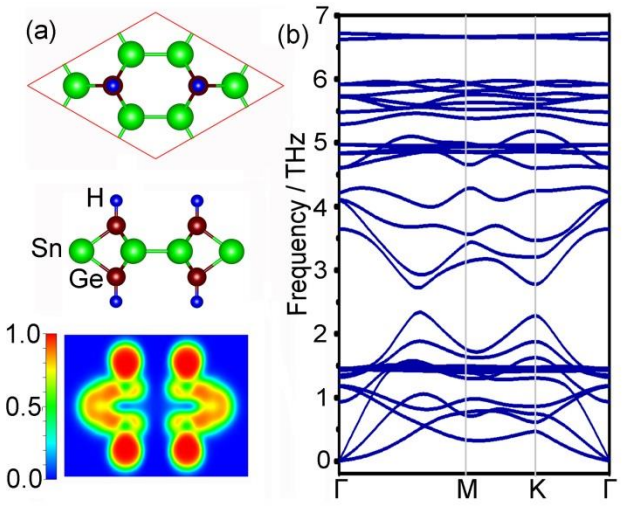

Figure 3. (a) Top (top panel) and side views (middle panel) and the ELF profiles (down panel) of a DB $Sn_6Ge_4H_4$ unit cell. (b) Phonon spectrum of DB $Sn_6Ge_4H_4$ along the high-symmetric points in the BZ.

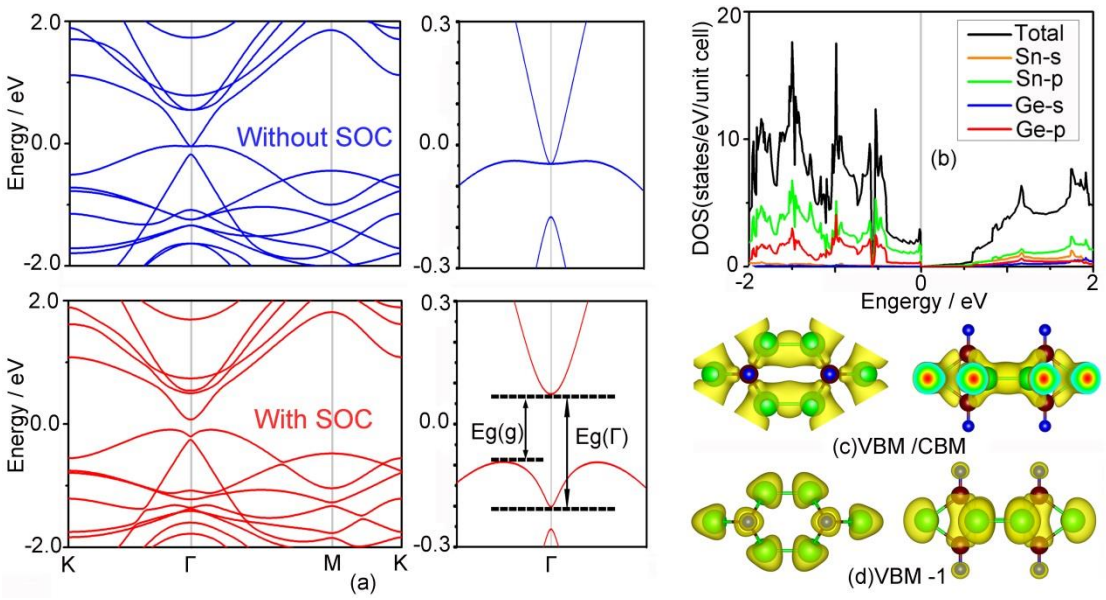

Figure 4. (a) The band structures without (top panel) and with SOC (down panel) of DB $Sn_6Ge_4H_4$, with their enlarged views of band lines shown in the right panel. (b) Orbital-resolved electron density states of DB $Sn_6Ge_4H_4$ without SOC. The DOS data were obtained by integrating the whole BZ. (c) and (d) are the isosurfaces of the electron wavefunctions of the VBM and VBM -1 at the Γ point. The isosurfaces of the CBM at the Γ point atom resemble those of the VBM and thus are not presented. The energy of the Fermi level was set to zero.

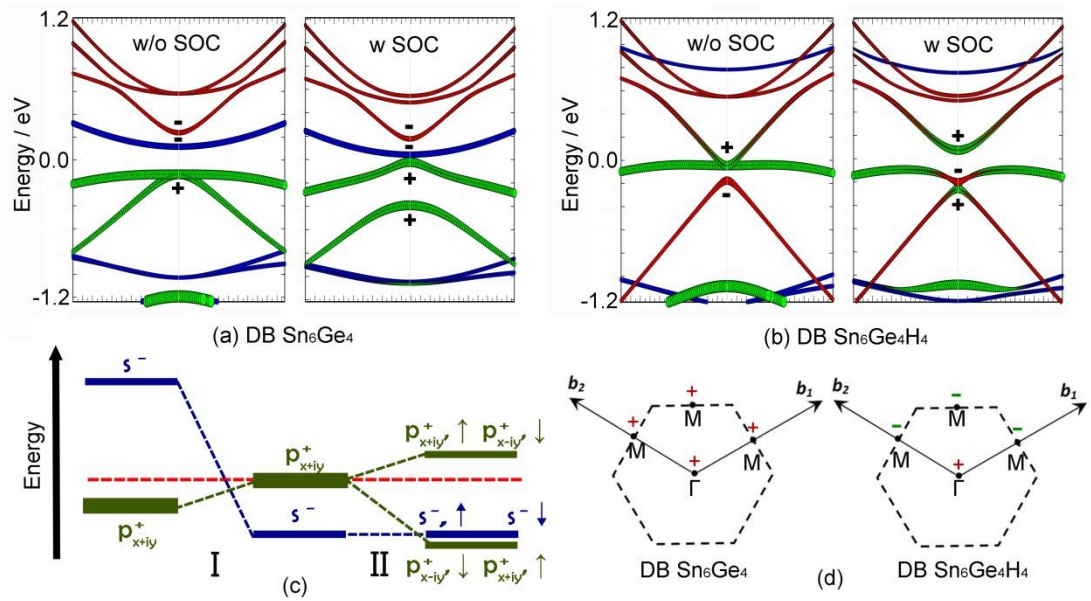

Figure 5. Comparison between the orbital-resolved band structures of (a) DB Sn_6Ge_4 and (b) DB $Sn_6Ge_4H_4$ in the vicinity of the Γ point obtained from DFT calculations without and with SOC. The superscript " + " and " – " denotes the parity of the wavefunctions. The contributions of different atomic orbitals are indicated by the dots in different colors and sizes. S-orbital of Sn (red), p_{xy}-orbital of Sn (green), and p_z-orbital of Sn (blue). (c) Schematic diagram of the electronic state evolution of DB Sn_6Ge_4 (left panel) and $Sn_6Ge_4H_4$ (middle and right panel) near the Fermi level. The red line denotes the Fermi level, and the effects of (I) hydrogenation and (II) SOC on the alignment of electronic states are indicated. (d) Brillouin zone of DB Sn_6Ge_4 and DB $Sn_6Ge_4H_4$. The signs (+/-) are associated with $\boldsymbol{\delta_i}$ at the time-reversal invariant momenta. b_1 and b2 are the primitive reciprocal lattice vectors.

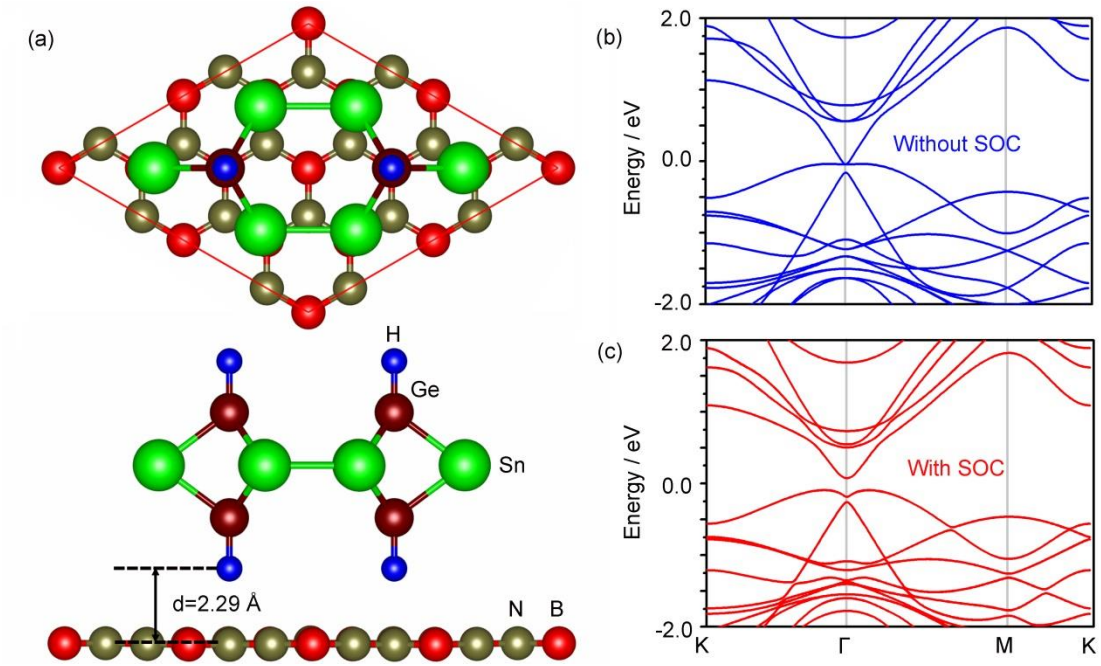

Figure 6. (a) Top and side views of a DB $Sn_6Ge_4H_4$ grown on a h-BN substrate. Electronic band structures of DB $Sn_6Ge_4H_4$ on h-BN substrate (b) without and (c) with SOC. The energy at the Fermi level was set to zero.